Changes in nuclei and peritumoral collagen within nodular basal cell carcinomas via confocal micro-Raman spectroscopy

Michael A. Short
Simon Fraser University
Department of Physics
8888 University Drive
Burnaby, British Columbia, V5A 1S6 Canada

Harvey Lui
University of British Columbia
Department of Dermatology and Skin Science
835 West Tenth Avenue
Vancouver, British Columbia, V5Z 4E8 Canada
and
British Columbia Cancer Research Centre
Cancer Imaging Department
675 West Tenth Avenue
Vancouver, British Columbia, V5Z 1L3 Canada

David McLean
University of British Columbia
Department of Dermatology and Skin Science
835 West Tenth Avenue
Vancouver, British Columbia, V5Z 4E8 Canada

Haishan Zeng
British Columbia Cancer Research Centre
Cancer Imaging Department
675 West Tenth Avenue
Vancouver, British Columbia, V5Z 1L3 Canada

Abdulmajeed Alajlan
University of British Columbia
Department of Dermatology and Skin Science
835 West Tenth Avenue
Vancouver, British Columbia, V5Z 4E8 Canada
and
King Faisal Specialist Hospital and Research Centre
Department of Medicine
Riyadh, Saudi Arabia

X. K. Chen
Simon Fraser University
Department of Physics
8888 University Drive
Burnaby, British Columbia, V5A 1S6 Canada
E-mail: mxchen@sfu.ca

Abstract. Confocal micro-Raman spectroscopy is used to probe the nuclei of normal human epidermal cells and epidermally derived cancer cells from nodular basal cell carcinomas. Clear differences are seen between the spectra. The nuclei of tumor cells appear to have different contributions from nucleic acids, histones, and proteins with an actin-like spectrum than those of normal epidermal cells. Changes in the contribution of DNA to the spectra are consistent with the staining of conventional histopathologic specimens. We also obtain spectra of the dermis, where it is found that the dermis close to tumor boundaries is not simply deficient in collagen, but shows signs of structural changes as well. © *2006 Society of Photo-Optical Instrumentation Engineers.* [DOI: 10.1117/1.2209549]

Keywords: basal cell carcinoma; Raman spectroscopy; nucleic acid; histones; actin; collagen; gelatin.

Paper 05152R received Jun. 24, 2005; revised manuscript received Dec. 9, 2005; accepted for publication Jan. 3, 2006; published online Jun. 6, 2006.

1 Introduction

Skin cancers are the most common malignancy diagnosed in Canada and the United States, with similar incidence rates between the two countries, and a combined total of more than 1 million new cases annually.[1,2] Furthermore, rates are expected to increase as the ozone layer thins and as members of older generations, to whom sunbathing became fashionable, age. Basal cell carcinomas (BCC) account for the majority (80%) of skin cancer cases,[3,4] with the nodular form of BCC being the most common. The disease most likely originates within pluripotent cells of the epidermis or epidermally derived follicular structures.[5] As the neoplastic cells multiply, they infiltrate and degrade the dermis using matrix metalloproteinases, the overall process of which is believed to play a key role in determining the aggressiveness of tumor invasion.[6–10] BCC is generally slow growing and rarely metastasizes, but it can cause extensive local damage if left unchecked because of its invasive growth pattern. Since there is

Address all correspondence to X. K. Chen, Physics, Simon Fraser University, 8888 University Drive, Burnaby, British Columbia V5A 1S6 Canada; Tel: 604 291 3160; Fax: 604 291 3592; E-mail: mxchen@sfu.ca

1083-3668/2006/11(3)/034004/9/$22.00 © 2006 SPIE

a strong correlation between the amount of sunlight exposure (especially during childhood) and BCC incidence, research on gene mutations due to UV damage is important (see Ziegler et al.[11]). Genetic studies have also been helpful because of the link between BCC and the hereditary disease, Gorlin syndrome (nevoid basal cell carcinoma syndrome).[12] Research on simple, noninvasive methods to detect BCC is important because, like all cancers, early detection results in a better prognosis. Several detection methods have been tried, but none have proven to be sufficiently reliable for clinical diagnosis.[13–15]

Micro-Raman spectroscopy is one tool that could provide useful insights on the pathophysiologic mechanism of skin cancers including BCC, and may help in the development of a rapid Raman-based clinical detection and evaluation tool. The method involves focusing high intensity, monochromatic light onto microscopic structures within tissue samples and collecting the inelastically scattered light (see Tu[16]). The change in frequencies of the scattered photons are correlated to vibrations of the molecules being excited, and thus provides a means to quantify their abundance and changes to their structure. Since diseased tissue has a different molecular composition than normal tissue, it may have a detectably different Raman spectrum, as has been shown for a variety of diseases (see Hanlon et al.[17]). One can empirically use changes in spectral shape or intensity (i.e., fingerprinting) to differentiate between samples, or in principle, actually identify the specific molecular changes that have occurred. In conventional Raman spectroscopy, where a relatively large diameter excitation beam is used, molecules are excited simultaneously from many different microstructures within the skin.[18] This is a problem, since most biological molecules have Raman emissions over similar ranges (400 to 1800, and around 3000 cm^{-1}), which makes it difficult to isolate changes in microstructures that contribute only a small fraction to the total Raman signal. Micro-Raman spectroscopy alleviates this difficulty, giving more precise spatial information as to where the molecular changes have occurred.

Micro-Raman spectroscopy is not without its experimental difficulties. The power density must be kept below a certain critical value so as not to damage the tissue structures.[19] This may mean spectra have to be accumulated over long integration times, which can be unacceptable, especially if they are to be acquired *in vivo*. Identifying similar microstructures to compare their Raman spectra can also be problematic. Despite these difficulties, Caspers, Lucassen, and Puppels[20] used micro-Raman spectra to identify different skin layers both *in vitro* and *in vivo*. Some success has also been obtained in probing single cells and correlating spectral variations with their biological differences (see Uzunbajakava et al.,[19] Puppels et al.,[21] Xie and Li,[22] and Notingher et al.[23]). Thus, there are good prospects for identifying molecular change from similar measurements on cells and other microstructures of skin diseased with BCC.

In 2002, Nijssen et al.[24] used micro-Raman spectroscopy with an excitation spot diameter of around a micrometer to obtain spectra with a 8 cm^{-1} resolution from thin sections of BCC. However, they scanned the sample over a 10×10-μm area during the data acquisition, so the spectra are effectively averages of 100-μm^2 areas. Furthermore, there was no attempt to identify each spectrum with a precise location in the sample other than broadly defined regions (e.g., epidermis, dermis, tumor, etc.). Nevertheless, the average spectra from these regions showed clear changes in DNA and collagen density. Given these promising results, it is possible that even more information on the pathophysiology of BCC may be obtained if spectra from known micrometer diameter sites in normal and diseased tissue are compared without averaging over larger areas. This information may also be of benefit for the development of a rapid, Raman-based diagnostic tool. We therefore embarked on an exploratory program to obtain such spectra. A spectrometer with a 2 cm^{-1} spectral resolution was used, since molecular changes can result in small changes in the Raman spectra not detectable at lower resolutions. We show the spectra of normal and malignant cell nuclei, and from points in the dermis at different distances from a tumor.

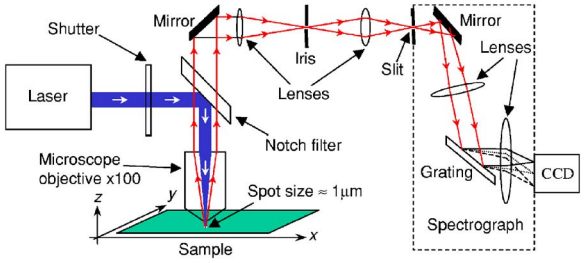

Fig. 1 Schematic showing the LabRam system for taking micro-Raman spectra. Not shown are the extra components needed to take white light images of the sample, which allow one to select different sites and focus laser beams onto them. The pairs of solid, dotted, and dashed lines emanating from the grating and converging at the CCD represent rays of dispersed light with decreasing frequency, respectively.

2 Methods and Materials

2.1 *Ethical Approval*

This research was approved by the Research Ethics Board at the Office of Research Ethics, Simon Fraser University, Burnaby, British Columbia, Canada.

2.2 *Raman Instrumentation*

Visible images and micro-Raman spectra were obtained with a LabRam (Jobin Yvon Incorporated, Edison, New Jersey) system, which consists of a He:Ne laser and a grating spectrograph coupled to an Olympus BX40 microscope (Fig. 1). The BX40 functions as a normal microscope, allowing positioning of the sample and capturing of visible images using a built in charge-coupled device (CCD) camera. The laser beam was focused onto the sample using a $100\times$ long working distance objective with a numerical aperture of 0.8. The diameter of the excitation spot at the sample was estimated to be approximately 1 μm at 10% of the maximum excitation intensity, and the maximum excitation power at the sample was 3 mW. Light scattered by the sample is collected by the same objective lens and passed through a notch filter, which blocks light at the same frequency as the incident light (i.e., elastically scattered light). The in-elastically scattered light passes through the notch filter and is brought to a focal point at the plane of an iris with an adjustable diameter of between 0 to 1200 μm. The latter allows in-elastically scattered light

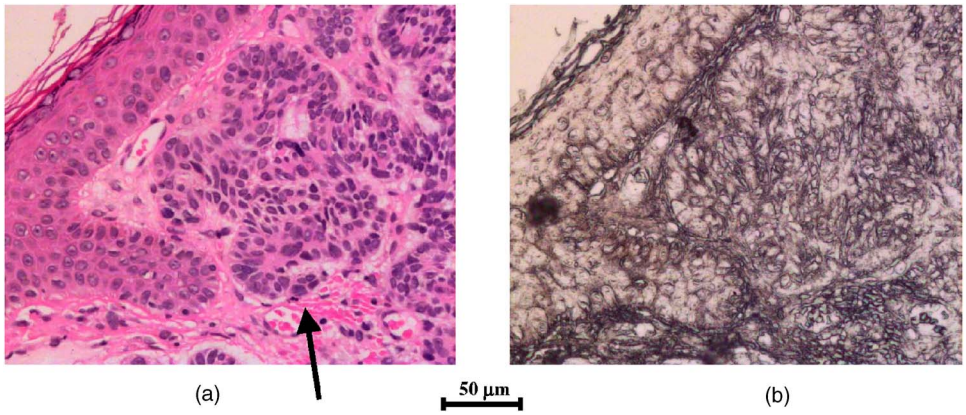

Fig. 2 Images of approximately the same location on two consecutive thin sections from BCC sample **A**. (a) is a deparaffinized and H and E stained section, and (b) is a deparaffinized but unstained section. In (a), one can clearly see the stratum corneum, cells in the epidermis, and the demarcation of the latter with the dermis. The arrow points to a cluster of malignant cells in the dermis. Most of the microstructures seen in (a) can also be seen in (b) apart from the tumor cells, which are more difficult to make out.

to be collected from layers of different thickness of a translucent sample, which gives the instrument a confocal capability. After passing through the iris, the in-elastically scattered light is focused onto the entrance slit of a spectrometer containing a choice of two holographic gratings. For all the spectra presented here, the slit width was set to 150 μm, and a 1800-g/mm grating was used. The intensity of the dispersed light was measured with a second CCD array cooled to $\approx -60\,^{\circ}$C to reduce the noise.

The frequency dispersion of the Raman system was calibrated by measuring the spectrum of a cyclohexane standard and then adjusting both the rotation of the grating and the CCD pixel to wave-number settings until the position of the Raman peaks matched those found by others.[25] The spectral resolution of the system was close to 2 cm^{-1}, as stated by the manufacturer for the settings used. The intensities of the Raman peaks obtained with the system were not corrected for the instrument response. Tests were undertaken on the system to determine the best signal-to-noise ratio (SNR) and depth of field by measuring the spectra of different sized calcite flakes placed on a silicon substrate. The optimum SNR for a calcite flake with a diameter of approximately 1 μm was found to occur when the iris diameter was set to 200 μm, consistent with that of similar systems.[26] Checks were made for any changes in sensitivity of the equipment or laser power during the experiments by measuring the Raman spectrum of the same site on a calcite flake after every 1000 s of operation. No significant changes in the intensities of the calcite peaks were seen over 1000 s of operation, although there were small fluctuations (a few percent) over many hours of operation. All spectra were corrected for these small fluctuations by scaling them up or down as appropriate.

2.3 *Sample Preparation*

Archival histopathologic tissue samples of three separate confirmed human nodular BCCs (**A**, **B**, and **C**) were obtained for analysis by micro-Raman spectroscopy. The samples had been processed immediately after excision by fixation with 10% formalin, followed by conventional histopathologic techniques and then embedded in paraffin wax. For this present work, two consecutive thin sections approximately 10 μm thick were cut from each archival sample. The sections were dewaxed by washing in xylene for 3 min, followed by a series of graduated alcohols (70 to 100%) for 3 min and then distilled water. Note that although this dewaxing procedure is likely to leave some residue, stronger treatments were avoided, as these may damage the samples.[27] One section was stained with hematoxylin and eosin (H and E), washed in distilled water, and mounted on a glass slide with a cover slip; these served as orientation slides to assist in positive identification of structures. The other section, from which the Raman measurements were taken, was left unstained and mounted on BaF_2 slides without a cover slip. BaF_2 slides were used instead of ordinary glass to avoid the large fluorescence background emitted from glass during laser excitation.

Figure 2 shows two images of sections from BCC sample **A** 20× magnification, and Fig. 3 are two images of the same sample at 100×. Images from the two other BCC samples **B** and **C** (not shown) were similar in appearance to those of **A**.

2.4 *Selection of Sites for Micro-Raman Analysis*

It was generally easy to identify the epidermis, dermis, and tumor regions in the stained sections. The cells within these regions and their nuclei and nucleoli could be easily seen. Cells, nuclei, and nucleoli could also be seen in the unstained sections. We used the stained sections to identify which cells in the unstained sections were from tumors and which were from disease-free regions. Micro-Raman spectra were then obtained from the unstained sections for both the nucleoli, and from intranuclear points immediately adjacent to them for both tumor cells and normal epidermal cells. For the connective tissue, we took spectra from the unstained sections from points close ($\leq$10 μm) to obvious tumor boundaries and also at greater distances ($\geq$100 μm).

2.5 *Reference Spectra*

Reference spectra were measured for DNA purified from a human placenta, RNA purified from baker's yeast, types H1 and Hm histones purified from a calf thymus (Hm is a heterogeneous mixture of types H1, H2a, H2b, H3, and H4), rabbit

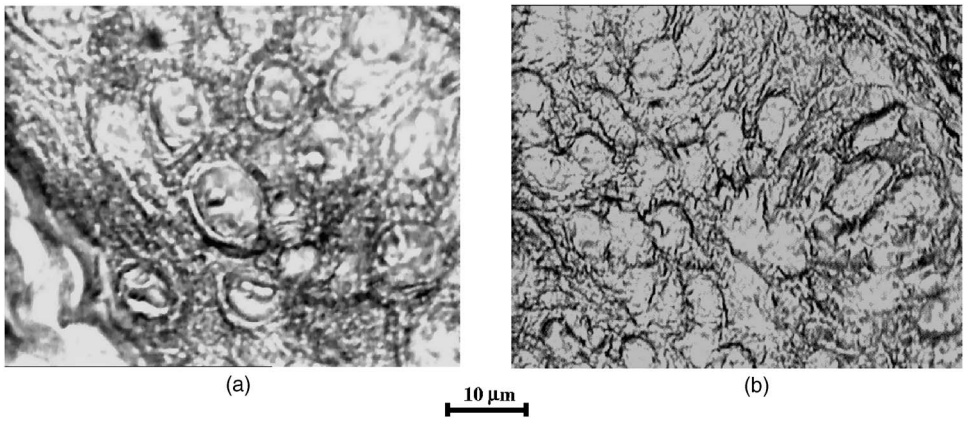

Fig. 3 High magnification images from two different regions of a deparafinnized, but unstained, thin section of BCC sample **A**. (a) is from a region in the epidermis and (b) is from a tumor cell nest in the dermis. One can clearly see gross features of the cells in (a), namely the cell outlines, and large nuclei ($\approx 8\ \mu m\varnothing$) containing nucleoli ($\approx 1\ \mu m\varnothing$). Similar cellular features can be barely discerned in (b).

muscle actin, type 1 collagen and elastin purified from bovine tendon, and unprocessed human stratum corneum (the latter is known to be 80% keratin by dry weight[28]). The first seven references were obtained from Sigma-Aldrich Canada Limited (Oakville, Ontario) with reference numbers D4642, R6750, H5005, H6005, A2522, C9879, and E1625, respectively. The stratum corneum was a 2-mm sized skin scale collected from a volunteer. A paraffin wax spectrum was also obtained from the same paraffin wax as that used to embed the samples. These reference materials were measured neat in their supplied state without any further processing. For each reference material, a small quantity was placed on a BaF_2 slide and a Raman spectrum obtained in the same way as the thin skin sections described later.

2.6 *Micro-Raman Spectroscopy*

A Raman spectrum covering the whole fingerprint region (400 to 1800 cm^{-1}) could not be obtained as one continuous spectrum without sacrificing resolution by changing the grating to a lower g/mm ratio. Instead, two spectra were taken at each site of interest: one from 300 to 1250 and the other from 1150 to 2000 cm^{-1}. These spectra were concatenated into one spectrum by scaling the intensities of the latter until they matched the former in the overlap region. The procedure for obtaining data was to reduce the excitation power to 10^{-4} of its maximum value and then focus on some point of the sample; this was necessary because high powers saturated the CCD camera, making focusing difficult. After focusing, the excitation power was then returned to its maximum value and ten 100-s spectra were taken. This procedure was repeated for ten nucleoli and points adjacent to them from cells in the epidermis and from cells within a tumor, and for points in the dermis at different distances from a tumor boundary. An analysis of the ten, 100-s spectra from the same site (not shown) revealed very little temporal change, indicating that the molecular composition and structure had not changed, which is consistent with what others found using equivalent excitation power densities.[19] A mathematical average spectrum for each site was then calculated.

High intensity noise spikes in the average spectra (which were rare) were removed manually, and low intensity, high frequency, noise spikes were removed using a five-point Fourier transform. A CCD dark count of 1250 counts was subtracted off each average spectrum. Two-tailed Mann-Whitney U (MWU) tests were used to compare visibly similar spectra from different sites, and nonlinear regression was used to model the spectra with a combination of reference spectra and background terms. (Subroutines from the SPSS software package were used for both the MWU tests and the nonlinear regression.) The background terms consisted of a constant and two exponentials (i,j) of the form $I_{i,j}\exp(\pm\tau_{i,j}\nu)$, where $I_{i,j}$ and $\tau_{i,j}$ are fitting parameters and υ is the spectral frequency. The exponentials were included because the spectra tended to rise slightly and smoothly at low and high wave numbers due to the low frequency shoulder of the excitation light and fluorescence from the samples and/or the BaF_2 slides, respectively. The fitting procedure used a Levenberg-Marquardt algorithm to minimize the residual sum of squares, and was constrained to coefficients ≥ 0. The tolerance of the coefficients and the residual sum of squares was set at 10^{-8}. A standard error for each reference coefficient in a fit was calculated.

3 Results

The Raman spectra for the same microstructure (e.g., nucleoli of malignant cells) were very similar for the different samples. Thus, we chose to average the spectra from the different samples; these spectra are compared in pairs in Figs. 4 through 7. The data below 600 cm^{-1} are not shown because of excessive noise.

The nuclei spectra shown in Figs. 4 through 7 are broadly similar in shape and intensity. However, there are significant differences between the spectra; this is demonstrated by MWU tests, which were performed pairwise on the sets of spectra whose averages are shown in Figs. 4 through 7. The test probabilities dip below 0.05 at several points over the spectral range, which indicates that there is at least a 95% certainty that the two spectral sets being compared are different at these points. Although some of the difference maybe due to variations in paraffin wax residual and background components, there appears to be clear changes in the intensity

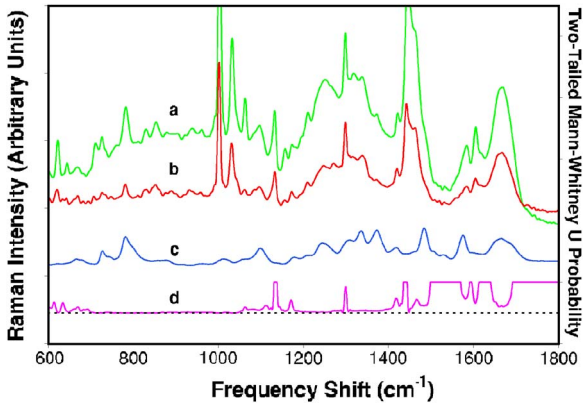

Fig. 4 Average Raman spectra from the nuclei of normal epidermal skin cells. Each spectrum is the average spectrum of 30 cells, ten from each sample. Also shown for comparison is the spectrum of the DNA reference. (a) Nucleoli, (b) points adjacent to the nucleoli, but still within the nucleus, (c) DNA reference, and (d) probability generated by the MWU test that compares the different sets of spectra that were used to calculate the average spectra (a) and (b). Note that the MWU probability has been truncated to a maximum of 0.05 for clarity, and the dashed line is at zero probability. Note that the closer the MWU probability is to zero, the greater the probability is that the two spectra are different at that frequency.

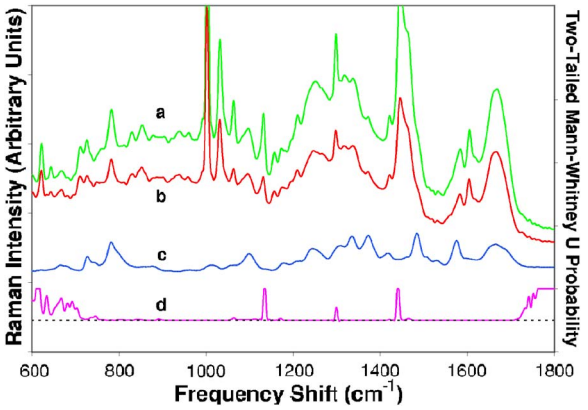

Fig. 6 Comparison of the average Raman spectra from the nucleoli of normal and malignant cells shown in Figs. 4 and 5. Each spectrum is the average spectrum of 30 cells, ten from each sample. Also shown for comparison is the spectrum of the DNA reference. (a) Nucleoli of normal epidermal cells, (b) nucleoli of BCC tumor cells, (c) DNA reference, and (d) probability generated by the MWU test that compares the different sets of spectra that were used to calculate the average spectra (a) and (b). Note that the MWU probability has been truncated to a maximum of 0.05 for clarity, and the dashed line is at zero probability.

of many of the other Raman peaks. The latter was confirmed by plotting the ratio of any two average Raman spectra (not shown), which resulted in plots with peaks and troughs coinciding with some of the Raman peaks.

The Raman spectra for five reference materials, RNA, histones (H1 and Hm), actin, and keratin, are shown in Fig. 8; the DNA spectrum was shown in previous figures. These reference spectra were used along with a paraffin wax spectrum and background terms to find the best fit to the skin nuclei spectra. An example of a typical fit is shown in Fig. 9. Note that although the fitting is reasonable considering the small number of reference spectra used, it does not completely account for the spectrum. Figure 10 shows the contribution to each fit of the different references (note that H1 and keratin both contributed a negligible amount to each fit and have thus been omitted from this plot).

As for the dermal spectra, three different types were identified from sites close to tumors; these are shown in Fig. 11. These spectra are each averages of ten sites from the dermis at approximately the same distance from a tumor in the dermis

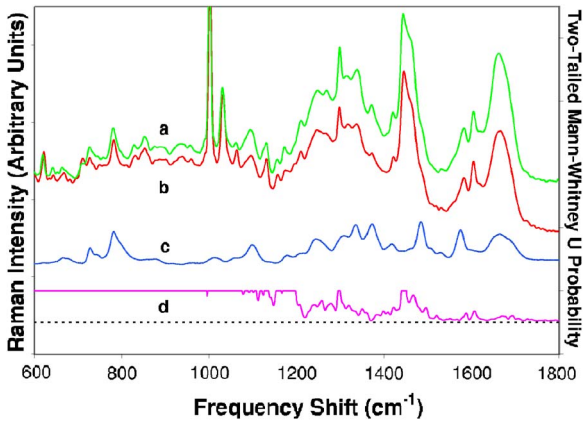

Fig. 5 Average Raman spectra from the nuclei of malignant cells within BCC tumors. Each spectrum is the average spectrum of 30 cells, ten from each sample. Also shown for comparison is the spectrum of the DNA reference. (a) Nucleoli, (b) points adjacent to the nucleoli, but still within the nucleus, (c) DNA reference, and (d) probability generated by the MWU test that compares the different sets of spectra that were used to calculate the average spectra (a) and (b). Note that the MWU probability has been truncated to a maximum of 0.05 for clarity, and the dashed line is at zero probability.

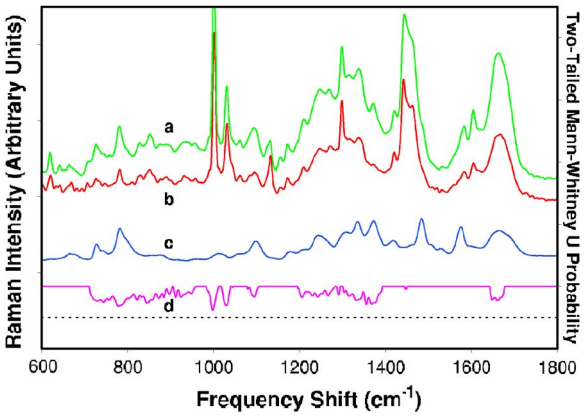

Fig. 7 Comparison of the average Raman spectra from points adjacent to the nucleoli of normal and malignant cells shown in Figs. 4 and 5. Each spectrum is the average spectrum of 30 cells, ten from each sample. Also shown for comparison is the spectrum of the DNA reference. (a) Normal epidermal cells, (b) BCC tumor cells, (c) DNA reference, and (d) probability generated by the MWU test that compares the different sets of spectra that were used to calculate the average spectra (a) and (b). Note that the MWU probability has been truncated to a maximum of 0.05 for clarity, and the dashed line is at zero probability.

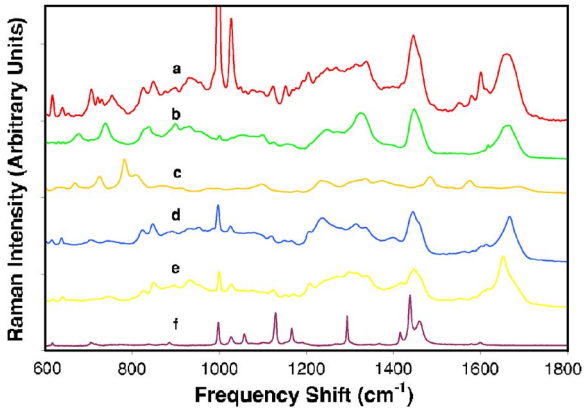

Fig. 8 Average Raman spectra from five references and paraffin wax. The spectra have been arbitrarily offset on the intensity scale for clarity. (a) Actin, (b) H1, (c) RNA, (d) Hm, (e) keratin, and (f) paraffin wax.

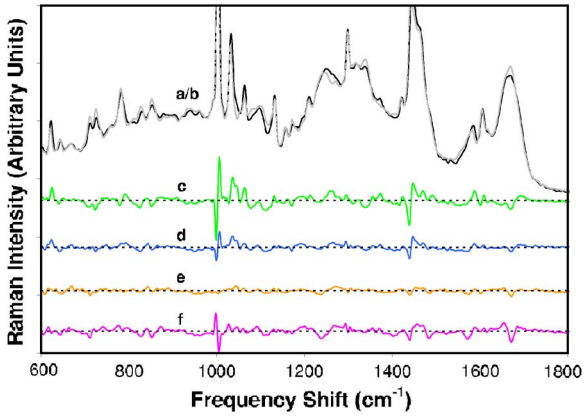

Fig. 9 Fit to the average Raman spectrum of nucleoli from normal epidermal cells with a combination of reference spectra, and residuals of the fit and of similar fits to other spectra. The spectra and residuals have been arbitrarily offset on the intensity scale for clarity. The dashed lines are at zero intensity. **a**/**b** is the average nucleoli spectrum of normal epidermal cells (dark line) and the fit to it (gray line), (c) residuals from the fit shown in **a**/**b**. (d) residuals from the fit (not shown) to the average BCC nucleoli spectrum, (e) residuals from the fit (not shown) to the average spectrum of points adjacent to the nucleoli of normal epidermal cells, and (f) residuals from the fit (not shown) to the average spectrum of points adjacent to the nucleoli of BCC cells.

of one sample. Dermal spectra from the other two samples were similar. Also shown in Fig. 11 are the collagen and elastin reference spectra.

4 Discussion

Our cell spectra (Figs. 4 through 7), apart from the presence of paraffin wax peaks (described later), were qualitatively similar to spectra obtained by others for similar samples.[20,23,24,29] We note here that fresh samples were used in the work presented in some of the latter references; thus it would appear that our sample processing did not have a great effect on the Raman emission consistent with what others have found for gentle fixing and dewaxing treatments.[27,30] As expected, there appears to be a significant DNA contribution to each spectrum. The main differences between our spectra and those obtained by Nijssen et al.[24] for BCC tumor and epidermis regions appear to be much less keratin and more nucleic acids in ours; this is presumably because our experimental setup and site selection minimizes the extra cellular contributions. The broad peaks centered near 1450 and 1670 cm^{-1} in our spectra are assigned to CH_2 bending and amide I vibrations, respectively, of lipids and proteins.[31] Peaks in the range 1200 to 1300 cm^{-1} are assigned to amide III vibrations, and those between 850 to 950 cm^{-1} to protein backbone vibrations. The sharp peaks near 1062, 1130, 1296, and 1441 cm^{-1} were most likely due to a paraffin wax residual in the samples.[27] Other small paraffin wax peaks may also be present at 1002, 1031, 1417, and 1463 cm^{-1}, but these coincide with other larger peaks, and thus it is not clear what their contribution is. Raman emission from amino acids phenylalanine and tyrosine are most likely the major contributors to the peaks near 623, 644, 1002, 1031, and 1600 cm^{-1}.

The MWU tests comparing our spectra of nuclei from normal and tumor cells showed there were significant variations. This was encouraging, since the most likely explanation is that these variations reflect molecular differences, which is exactly the information we are interested in. Differences between the spectra of nucleoli and sites adjacent to them are presumably related to their different biological functions.[32] In contrast, one does not expect differences between similar sites from cells of the same type. We therefore interpret the differences between the Raman spectra of normal and tumor cells being due to molecular changes caused by disease. Although the MWU plots indicate that molecular changes have occurred between different cells, it is not visually obvious as to what these changes are. Furthermore, it was impossible to identify frequency shifts or changes in shape of any of the Raman peaks that were due to molecular damage as opposed to changes in molecular composition. Thus, it would appear that a 2-cm^{-1} resolution spectrograph does not yield any additional useful information than one with a lower resolution, although in cases where the Raman intensity is higher, high spectral resolution may still be advantageous.

The modeling of our nuclei spectra with the reference spectra (Fig. 9) was successful in that the fitting accounted for the main spectral features, and were comprised of significant contributions from nucleic acids and histones [Figs. 10(a) and 10(b)]. The complete absence of a keratin component in any of the fits presumably reflects the fact that keratin fibers are only present in significant amounts outside the nuclei of epidermal keratinocytes.[32] This conclusion is supported by the observation of a dominant keratin component in spectra (not shown) taken from locations outside the nuclei of epidermal cells. Nucleoli from normal cells showed greater RNA, histone, and actin contributions compared with the rest of the normal nucleus, but similar DNA contributions [Fig. 10(a)]. Although Fig. 10(b) shows, as percentages of the total emission, that DNA and histones are in fact less in the normal nucleoli. Thus, normal nucleoli give more intense Raman spectra, which have proportionally more RNA and actin but less DNA and histones than the rest of the nuclei. More RNA in the nucleoli is consistent with its known functions; however, we could find no support in the literature for a greater actin contribution. Until quite recently, even the presence of

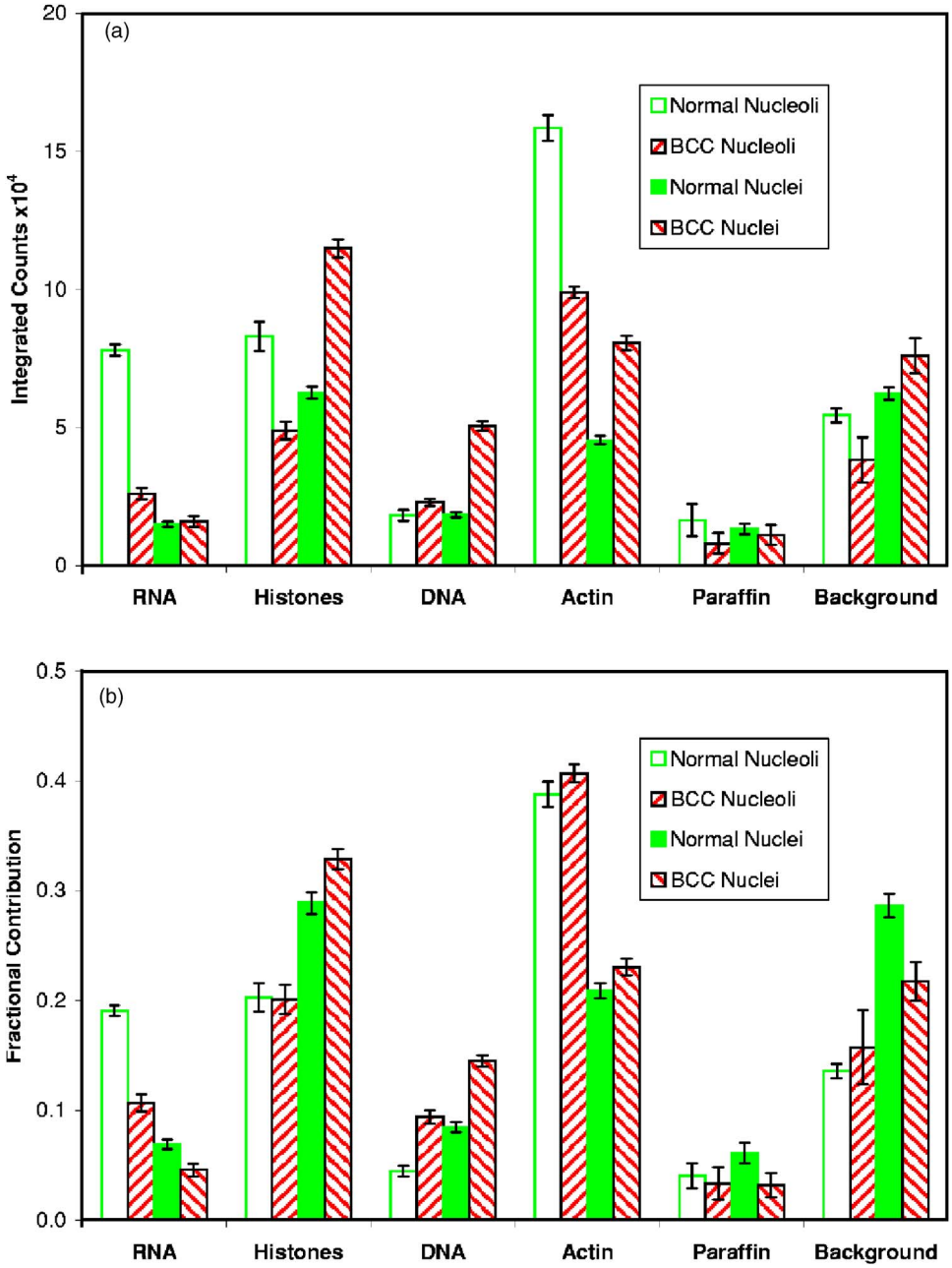

Fig. 10 Contribution of each reference spectrum, paraffin wax, and background terms that best accounts for the spectra shown in Figs. 4 through 7. In (a), the total number of counts under the curve of each reference spectrum and the background terms used in a fit are shown, and in (b) the same data are shown as in (a), but normalized to the total number of counts of all the contributions used in a fit. The error bars are the standard errors for each of the components in a fit. The background terms used in the fits consisted of a constant and two exponentials (i,j) of the form $I_{i,j}\exp(\pm\tau_{i,j}\nu)$, where $I_{i,j}$ and $\tau_{i,j}$ are fitting parameters and ν is the spectral frequency.

actin in the nucleus was controversial,[33] but now it seems to be clearly associated with many processes, and some of these occur in the nucleolus. Thus, our observation of an increased actin contribution in the normal nucleolus as compared to the rest of the nucleus is a distinct possibility.

The modeling of spectra from tumors cells did not show the same component contributions as the spectra from normal cells. Our spectra indicate that the molecular composition of both the nucleoli and the rest of the nuclei of tumor cells have changed. The nucleoli from tumor cells had smaller amounts of RNA, histones, and actin than nucleoli from normal cells [Fig. 10(a)]. Conversely, the nuclei of tumor cells had greater DNA, histone, and actin contributions than the nuclei of normal cells. This change is not simply due to changes in the intensity of spectra, because Fig. 10(b) shows that while the percentage of histones and actin remains similar between normal and tumor cells, large changes in nucleic acids have occurred. A greater DNA content in the nuclei of tumor cells is consistent with the H and E stained sections, which show nuclei of tumor cells appearing uniformly dark without clear

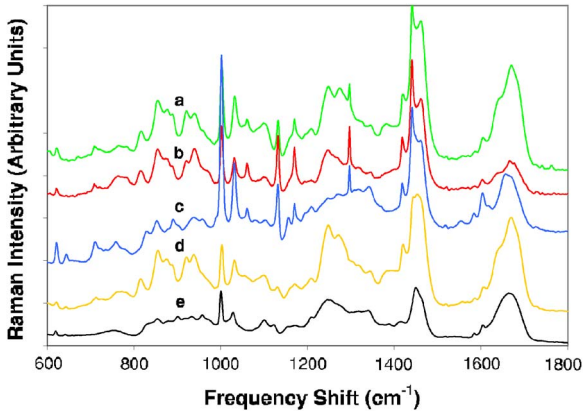

Fig. 11 Raman spectra from the dermis close to a tumor and the collagen and elastin reference spectra. Each spectrum is an average of ten sites approximately the same distance from a tumor in the dermis of one of the samples. The spectra have been arbitrarily offset on the intensity scale for clarity. (a), (b), and (c) are examples of the different types of spectra obtained from sites close to tumors. (d) is the collagen reference spectrum, and (e) is the elastin reference spectrum.

nucleoli, whereas normal epidermal cells show dark nucleoli within a paler nuclei. A larger histone contribution in the nuclei of tumor cells is also consistent with a larger DNA contribution, given the close relationship between them. We do not have a complete physiological explanation for these observations yet, other than that they are caused by disease. The fact that the modeling did not result in perfect fits shows there are still some minor molecular components missing; this is not surprising, since there are more than 270 proteins in a nucleolus alone.[34] More work is required to determine which proteins will make the best improvements to the fits.

Our spectra of the dermis around tumors again show sharp paraffin wax peaks as described before (Fig. 11) superimposed on a number of broad peaks. There are significant variations in the spectra that cannot be explained by variations in a paraffin wax residual. The spectra could be grouped into three types: spectra **a** and **b** look like that of the collagen reference spectrum **d**, except that spectrum **b** has a significantly larger peak near 940 cm^{-1}, and the peaks near 1210 and 1275 cm^{-1} are much reduced. Spectrum **c** on the other hand looks completely different from either collagen or elastin (the main fibrous components of the dermis), but is similar to an actin spectrum (see Fig. 8). Although Nijssen et al.[24] did report changes in the dermis spectra close to tumors, the changes seemed to be largely in intensity rather than shape. The discrepancy between their spectra and ours was probably due to their averaging process, which grouped signals from larger areas together. Spectra from sites in the dermis far from any tumor were indistinguishable from that of the collagen or elastin references, and therefore were not shown in Fig. 11.

It is well known that collagen is degraded in various stages by the action of collagenase secreted by malignant cells.[6–10] Frushour and Koenig[35] found the difference between the Raman spectra of collagen and thermally denatured collagen (gelatin) was an increase in the peak near 940 cm^{-1} and a reduction in the peak near 1210 cm^{-1}, consistent with our data. However, they did not show significant changes to the peak near 1270 cm^{-1}. They proposed that the latter was due to amide III vibrations at proline poor regions of the alpha chains, which are largely uneffected by thermal collagen-gelatin transitions. This is consistent with the results of Dong et al.,[36] who found that the peak near 1270 cm^{-1} in collagen could only be completely destroyed by heating the sample to 110°C, which is much higher than the collagen-gelatin transition temperature (37°C). Collagenase on the other hand does not merely cause an unwrapping of the collagen alpha chains, it cuts them into 0.75 and 0.25 fragments, leaving them susceptible to further degradation by gelatinases. Thus, one might expect the Raman spectrum of collagenase-degraded fibers to be similar to that of gelatin but with absence of some peaks. This would explain our dermal spectrum (curve **b**, Fig. 11).

As for the actin-like spectra (curve **c**), we can think of two possible explanations. One is that they may be due to actin microfilaments that spread out from the tumor into the surrounding dermis to aid invasion and cell motility.[37] Recall that our spectra from the nuclei of tumor cells showed a significant increase in actin density; we suggest that this may be connected with tumor invasion. Alternatively, but less likely, is that the spectra represent collagen in a more advanced stage of degradation. More work is needed to confirm or reject these hypotheses.

5 Conclusion

We show that there are clear differences in the micro-Raman spectra at a 1-μm spatial resolution between the nuclei of normal epidermal and BCC cells, and between spectra of the dermis at different distances from a tumor. The nucleoli from tumor cells has less RNA, histones, and actin than nucleoli from normal cells, whereas the rest of the nucleus from tumor cells has more DNA, histone, and actin than the nuclei of normal cells. There were other small changes between spectra of normal and diseased cells that are unidentified. A variation in the shape of spectra from the dermis near tumors is also identified. This is interpreted as being due to either collagen degradation or presence of tumor-induced actin microfilaments. In summary, we show that micro-Raman spectroscopy has good potential for probing information on molecular changes caused by BCC, which will help in understanding its pathophysiologic mechanism, and may help in the development and interpretation of Raman spectroscopy as a noninvasive diagnostic method.

Acknowledgments

This work was supported by the National Science and Engineering Research Council of Canada, the National Cancer Institute of Canada, with funds from the Canadian Cancer Society and the Canadian Dermatology Foundation.

References

1. Canadian Cancer Society, National Cancer Institute of Canada, Statistics Canada, Provincial/Territorial Cancer Registries, and Health Canada, *Canadian Cancer Statistics 2004*, Canadian Cancer Society, see http://www.cancer.ca (2004).
2. American Cancer Society, *Cancer Facts & Figures 2004*, American Cancer Society, see http://www.cancer.org (2004).
3. R. P. Gallagher, B. Ma, D. I. McLean, C. P. Yang, V. Ho, J. A. Carruthers, and L. M. Warshawski, "Trends in basal cell carcinoma, squamous cell carcinoma and melanoma of the skin from 1973 to 1987," *J. Am. Acad. Dermatol.* **23**, 413–421 (1990).

4. R. Marks, "The epidemiology of non-melanoma skin cancer: who, why what can we do about it," *J. Dermatol.* **22**, 853–857 (1995).
5. S. J. Miller, "Pathogenesis (basal cell carcinoma)," in *Cutaneous Oncology*, M. E. Maloney and S. J. Miller, Eds., pp. 581–585, Blackwell Science, Malden (1998).
6. E. D. Harris, C. S. Faulkner, and S. Wood, "Collagenase in carninoma cells," *Biochem. Biophys. Res. Commun.* **48**, 1247–1253 (1972).
7. E. D. Harris and S. M. Krane, "Collagenases (second of three parts)," *N. Engl. J. Med.* **290**, 605–609 (1974).
8. B. K. Pilcher, J. A. Dumin, B. D. Sudbeck, S. M. Krane, H. G. Welgus, and W. C. Parks, "The activity of collagenase-1 is required for keratinocyte migration on a type 1 collagen matrix," *J. Cell Biol.* **137**, 1445–1457 (1997).
9. J. Varani, Y. Hattori, Y. Chi, T. Schmidt, P. Perone, M. E. Zeigler, D. J. Fader, and T. M. Johnson, "Collagenolytic and gelatinolytic matrix metalloproteinases and their inhibitors in basal cell carcinoma of skin: comparison with normal skin," *Br. J. Cancer* **82**, 657–665 (2000).
10. L. Chung, D. Dinakarpandian, N. Yoshida, J. Lauer-Fields, G. Fields, R. Visse, and H. Nagase, "Collagenase unwinds triple-helical collagen prior to peptide bond hydrolysis," *EMBO J.* **23**, 3020–3030 (2004).
11. A. Ziegler, D. J. Leffell, S. Kunala, H. W. Sharma, M. Gailani, J. A. Simon, A. J. Halperin, H. P. Baden, P. E. Shapiro, A. E. Bale, and D. E. Brash, "Mutation hotspots due to sunlight in the p53 gene on nonmelanoma skin cancers," *Proc. Natl. Acad. Sci. U.S.A.* **90**, 4216–4220 (1993).
12. A. E. Bale and K. Yu, "The hedgehog pathway and basal cell carcinomas," *Hum. Mol. Genet.* **10**, 757–762 (2001).
13. M. Gniadecka, H. C. Wulf, N. Nymark-Mortensen, O. Faurskov-Nielsen, and D. H. Christensen, "Diagnosis of basal cell carcinoma by Raman spectroscopy," *J. Raman Spectrosc.* **28**, 125–129 (1997).
14. H. Zeng, D. I. McLean, C. E. MacAulay, B. Palcic, and H. Lui, "Autofluorescence of basal cell carcinoma," *Proc. SPIE* **3245**, 314–317 (1998).
15. R. Dua, D. G. Beetner, W. V. Stoecker, and D. C. Wunsch, "Detection of basal cell carcinoma using electrical impedence and neural networks," *IEEE Trans. Biomed. Eng.* **51**, 66–71 (2004).
16. A. T. Tu, *Raman Spectroscopy in Biology: Principles and Applications*, Wiley, New York (1982).
17. E. B. Hanlon, R. Manoharan, T. W. Koo, K. E. Shafer, J. T. Motz, M. Fitzmaurice, J. R. Kramer, I. Itzkan, R. R. Dasari, and M. S. Feld, "Prospects for *in vivo* Raman spectroscopy," *Phys. Med. Biol.* **45**, R1–R59 (2000).
18. P. J. Caspers, G. W. Lucassen, R. Wolthuis, H. A. Bruining, and G. J. Puppels, "*In vitro* and *in vivo* Raman spectroscopy of human skin," *Biospectroscopy* **4**, s31–s39 (1998).
19. N. Uzunbajakava, A. Lenferink, Y. Kraan, G. Volokhina, G. Vrensen, J. Greve, and C. Otto, "Nonresonant confocal raman imaging of DNA and protein distribution in apoptotic cells," *Biophys. J.* **84**, 3968–3981 (2003).
20. P. J. Caspers, G. W. Lucassen, and G. J. Puppels, "Combined in vivo confocal Raman spectroscopy and confocal microscopy of human skin," *Biophys. J.* **85**, 572–580 (2003).
21. G. J. Puppels, F. F. M. de Mul, C. Otto, J. L. Greve, M. Robert-Nicoud, D. J. Arndt-Jovin, and T. M. Jovin, "Studying living cells and chromosomes by confocal Raman microspectrometer," *Nature (London)* **347**, 301–303 (1990).
22. C. Xie and Y. Q. Li, "Confocal micro-Raman spectroscopy of single biological cells using optical trapping and shifted excitation difference techniques," *J. Appl. Phys.* **93**, 2982–2986 (2003).
23. L. Notingher, I. Bisson, A. E. Bishop, W. L. Randle, J. M. Polak, and L. L. A. Hench, "In situ spectral monitoring of mRNA translation in embryonic stem cells during differentiation in vitro," *Anal. Chem.* **76**, 3185–3193 (2004).
24. A. Nijssen, T. C. B. Schut, F. Heule, P. J. Caspers, D. P. Hayes, M. H. A. Neumann, and G. J. Puppels, "Discriminating basal cell carcinoma from its surrounding tissue by Raman spectroscopy," *J. Biomed. Opt.* **7**(1) 64–69 (2002).
25. J. M. Tedesco and K. L. Davis, "Calibration of dispersive Raman process analyzers," *Proc. SPIE* **3537**, 200–212 (1999).
26. G. J. Puppels, W. Colier, J. H. F. Olminkhof, C. Otto, F. F. M. de Mul, and J. L. Greve, "Description and performance of a highly sensitive confocal Raman microspectrometer," *J. Raman Spectrosc.* **22**, 217–225 (1991).
27. E. Ó Faoláin, M. B. Hunter, J. M. Byrne, P. Kelehan, H. A. Lambkin, H. J. Byrne, and F. M. Lyng, "Raman spectroscopic evaluation of efficacy of current paraffin wax section dewaxing agents," *J. Histochem. Cytochem.* **53**, 121–129 (2005).
28. P. M. Steinert and I. M. Freedberg, "Molecular and cellular biology of keratins," in *Physiology, Biochemistry and Molecular Biology of the Skin*, L. A. Goldsmith, Ed., pp. 113–147, Oxford University Press, New York (1991).
29. H. P. Buschman, G. Deinum, J. T. Motz, M. Fitzmaurice, J. R. Kramer, A. van der Laarse, A. V. Bruschke, and M. S. Feld, "Raman microspectroscopy of human coronary atherosclerosis: biomedical assessment of cellular and extracellular morphological structures in situ," *Cardiovasc. Pathol.* **10**, 69–82 (2001).
30. Z. Huang, A. McWilliams, S. Lam, J. English, D. I. McLean, H. Lui, and H. Zeng, "Effect of formalin fixation on the near-infrared Raman spectroscopy of normal and cancerous human bronchial tissues," *Int. J. Oncol.* **23**, 649–655 (2003).
31. B. G. Frushour and J. L. Koenig, *Raman Spectroscopy of Proteins*, Heyden, London (1975).
32. B. Alberts, *Molecular Biology of the Cell*, 2nd ed., Garland Publishing, New York (1989).
33. B. T. Bettinger, D. M. Gilbert, and D. C. Amberg, "Actin in the nucleus," *Nat. Rev. Mol. Cell Biol.* **5**, 410–415 (2004).
34. J. S. Andersen, C. E. Lyon, A. H. Fox, A. K. L. Leung, Y. W. Lam, H. Steen, M. Mann, and A. Lamond, "Directed proteomic analysis of the human nucleolus," *Curr. Biol.* **12**, 1–11 (2002).
35. B. G. Frushour and J. L. Koenig, "Raman scattering of collagen, gelatin, and elastin," *Biopolymers* **14**, 379–391 (1975).
36. R. Dong, X. Yan, X. Pang, and S. Liu, "Temperature dependent Raman spectra of collagen and DNA," *Spectrochim. Acta, Part A* **60**, 557–561 (2004).
37. M. W. Lee, S. J. Ahn, J. H. Choi, K. C. Moon, and J. K. Koh, "Actin and calponin expression in basal cell carcinoma," *Br. J. Dermatol.* **151**, 934–936 (2004).